The Role of Human Serum Albumin (HSA) in Modulating Aristolochic Acids (AA-I/II) Carcinogenicity

By: Ashley K.
University of Massachusetts Lowell
Crystallography and Structural Bioinformatics
Due: May 2nd, 2025
Grade: 88% (B+)

Abstract
This report reviews recent research provided in the research journal “Structural and Mechanistic Insights into the Transport of Aristolochic Acids and their Active Metabolites by Human Serum Albumin” by Karen Fleming and the members of the JBC Editorial Board. This is research important because while Aristolochic acids I and II (AA-I/II) are known carcinogenic principles of the Aristolochia plant, they may be used to treat several human conditions, chronic conditions, and may be used for the development of drugs/drug discovery. AA-I/II have long been used in traditional medicines despite being carcinogenic species but unfortunately AA-I is additionally a strong nephrotoxin. Since specifics into AA-I/II are not well known, structural and mechanistic information could lead to new medical treatments and medications to be discovered. The goal of the research was to investigate and identify the role of human serum albumin (HSA) in modulating AA-I/II carcinogenicity. This was studied by identifying the molecular forces governing the interactions between AA-I/II and their activated metabolites with human serum albumins and understand how the interactions transport toxic agents to tissues/organs in order to understand the metabolic pathways of AA-I/II and their mechanisms for distribution.

Methods used during the study include DNA adduct analysis, x-ray crystallography, isothermal titration calorimerty, and fluorescence quenching. Results of this study showed that HSA extends the half-life as well as reactivity of active metabolites of AA-I, HSA interactions with AA-I/II and their metabolites are modulated differently by the presence of fatty acids, association of AA-I/II with defatted HSA exibit2 binding sites, and identification and structural clarifications of AA-I/II interactions. The collective findings in the study show significant insight in the complex pathways of AA-I/II and how their carcinogenic effects as well as showing the role HSA has in reducing/increasing AA-I/II toxicity. These findings are an important step towards rational design, development, and implementation of future therapies and treatments by using the modulatory effect of non-toxic ligands to displace and detoxify active metabolite species.

Introduction

For centuries people all over the world have been using herbal remedies to cure their ailments, diseases, and chronic illnesses. A known plant used to cure people is the traditional Chinese and folk plant, the Aristolochia plant. The plant contains aristolochic acids (aka "AAs") and the plant generates various nitrophenantheren carboxylic acids and aristolactams. Some of these are known to be carcinogens and kidney toxins. Aristolochia's key carcinogenic species are AA-I (additonally has a dual role as a potent nephrotoxin) and AA-II. The mechanisms of AA-I's nephrotoxicity aren't well understood, however, it is understood that the carcinogenicity of AA-I/AA-II are associated with the formation of aristolactam(AL)-DNA adducts. These are highly mutagenic and they induce A to T mutations in a preferential manner in non-transcribed DNA strands that are in the 5'-CAG-3' motif. For DNA to bind covalently, AAs need an enzymatic activation, as seen in figure 1, below.

FIGURE 1- Aristolochic Acids with their bioactivation pathways

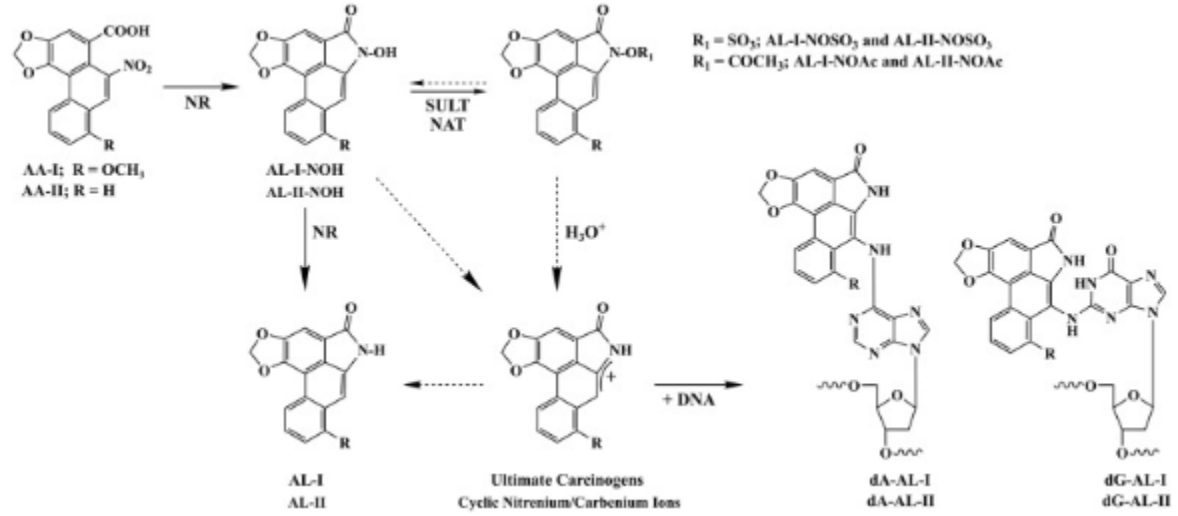

LEGEND: *Various enzymes (such as NQO1, CYPOR, XDH, and CYP1A/2) become responsible for nitroreduction (NR) of AA-I/AA-II. This in turn generates N-hydroxyaristolactams AL-I-NOH/AL-II-NOH. AL-I-NOH/AL-II-NOH are metabolites and may undergo additional NR forming the biologically inactive aristolactams AL-I/AL-II. The bioactivation through sulfonation catalyzed by sulfotransferases 1A1/1A2/1A3/1B1 (SULT) or through NO-acetylation by N-acetyltransferases ½ (NAT) produces AL-NOSO3 or AL-NOCAc species. The AL-I-NOSO3, AL-II-NOSO3, AL-I-NOAc, and AL-II-NOAc then will undergo heterolytic cleavage, which forms cyclic niternium/carbenium ions. The activated species are identical to those derived from decomposition of AL-I-NOH/AL-II-NOH but the latter are more stable than respective esters and will result in DNA adduction to occur at more reduced rates. Genotoxicity of AAs are associated with the formation of dA-(AL) and dG-(AL) aristolactam adducts. The dashes arrows represent non-enzymatic processes.*

When using an integrated human liver-kidney organs-on-chips method, it was demonstrated that human hepatic cells will produce the active metabolites of AA-I, which is distributed to the kidneys as well as a suspected array of organs. Renal and multiple cell types are able to generate active AA species, however, it seems as though the human liver cells greatly contribute to overall carcinogenic effects that are seen in diverse tissues. Plasma protein binding can impact distribution and effective toxicity of environmental

compounds aside from its vital role in the clearance and metabolic pathways. Human serum albumin (HSA) has a fundamental role in sequestering and transporting molecular species but there is a lack of reports that aim for the characterizing of binding of AAs to HSA. HSA has a single tryptophan residue (Trp214) that is in the IIA subdomain, serving as an intrinsic flourophore, this serves as a unique advantage. The analysis of ligand-induced fluorescence quenching profiles implies the formation of a complex where a single AA-I molecule will bind to HSA, assumingly in the IIA subdomain. This study helps address the lack of understanding through persing experimental strategies that integrates spectroscopic and calorimetric techniques to facilitate acquisition of the necessary AA:HSA parameters for binding.

Additional limitations in binding studies are the use of bulk commercial HSA preps from pooled human plasma. The preps frequently have a significant ratio of cross-linked species because there is a singular CySH34 (unpaired free thiol group) in the native HSA which is susceptible to several modifications (which include dimerization). Also, CySH34 is prone to covalent bonding with electrophilic species of different xenobiotics. The modified species of albumin will form crystals that tend to diffract poorly. There is also a lack of evidence regarding how the modifications will impact fluorescence quenching and/or ligand binding properties of the HSA Trp214. Around these limits, the study generated a mercaptoalbumin-reduced form of HSA when they incubated commercial protein samples in mild BME (beta-mercaptoethanol) conditions and using and applying a protocol successfully studying the adduction between albumins and carcinogens in vitro. A vast majority of published studies only focus on AA-I interactions with HSA and in turn poses the question of if AA-II shows similar binding properties. Additionally, prior to this study, there have been no high-res crystal structures reported for AAs bound to HSA and the characterization of the interactions between active labile AA-metabolites and HSA. The goal of the research was to investigate and identify the role of human serum albumin (HSA) in modulating AA-I/II carcinogenicity. The study demonstrates that AA-I/AA-II interactions with HSA can best be described as a two-site binding model where the resulting complexes are made up of two AA molecules that are bound to an HSA monomer. It is interpreted that the AA-I/AA-II binding parameters within the context of some specific interactions extracted through structural eludication of intermolecular contacts in AA-HSA complexes. These findings are important because the understanding of these mechanisms will lead to drug discovery and new treatments.

Materials and Methods

The following methods and materials are summarized from that of the procedures carried out during the research for the supplementary research journal "Structural and Mechanistic Insights into the Transport of Aristolochic Acids and their Active Metabolites by Human Serum Albumin". Procedures executed in this study include DNA adduct analysis, x-ray crystallography, isothermal titration calorimetry, and fluorescence quenching.

DNA Adduct Analysis

DNA was digested in a mixture containing 20mM sodium succinate (at a pH of 6), 8mM CaCl2, 0.8 units of micrococcal nuclease (staphylococcus aureus) from Sigma Aldrich, and 0.04 units of bovine spleen phosphodiesterase II from MP Biomedicals. Reactions proceeded overnight at 37C. After the digestion, 100mM of zinc chloride and 1 unit of nuclease P1 (penicillium citrinum) from MP Biomedicals were added and mixtures incubated at 37C for 1 hour. For the standard curves, synthetic oligonucleotides containing one dA-AL-II or dG-AL-II at the center of their respective 24-mer sequences were then digested as a mix of 15 fmol, 30 fmol, and 60 fmol and parallel processed with DNA samples. The digestion mixes of synthetic standards additionally included unmodified ssDNA . Adducted 3'-phosephate nucleosides were briefly enriched with two rounds of butanol extraction, dried under a vacuum, and 5'-labelled when in the presence of gamma32P-ATP from PerkinElmer and polynucleotide kinase lacking 3'-phosphatase activity from New England Biolabs. The labeled samples were run in SDS PAGE where the SDS gels were the gels were exposed to a GE Healthcare phosphor screen for 1 hour and 15 minutes (75 minutes) and overnight. A Typhoon system and densitometry conducted using Molecular Dynamics (Image QuaNT) were used in order to visulaize results. AL-DNA adduct levels (as a sum of dG-AL-I and dA-AL-I) were plotted against incubation times of the AL-I-NOSO3 prior to DNA addition. The AL-DNA levels were offered as mean values and standard deviations in the Sigma Plot (SPSS Inc) generated graphs.

Flourescence Quenching

The equilibrium fluorescence spectra of monomeric HSA samples were obtained on an ISS PCI photon counting spectrophotometer. The wavelength used was 295 nm, which is an excision wavelength, was used for HSAA3782 and HSAA8763 in order to selectively monitor tryptophan and to avoid tyrosine residue contributions. Excitation and emission slits were set at 1 and 2 nm. Before initiating the experiment, stock solution of each AA compound (AA-I/AA-II, AL-I-NOH/AL-II-NOH, and AL-I-NOSO3) was prepped in DMSO via serial dilutions to a 100-fold excess of final concentrations used in the quenching experiments. The HSA samples used were diluted to 0.5uM, 1.0uM, and 2.5uM in 10mM KPi buffer (with a pH of 7.5) then were divided into 1mL portions in eppendorf tubes. Portions of each AA compound were added to these HSA solutions in order to obtain a 0.2uM to 50uM concentration range in 1% DMSO. The AA-HSA mixtures were equilibrated for 5 minutes at room temperature then transferred to a 10mm x 5mm quartz cuvette, and the emission spectrum was recorded over wavelength range 310nm to 460nm and using a 2nm step interval. Peak emission intensities at 340nm were used to create fluorescence titration profiles for each of the AA compounds.

These fluorescence titration profiles of the HSA quenching assays are created using SigmaPlot. To compare HSA preps across AA ligands, a nonlinear equation that doesn't specifically consider several site

binding was used and provides great insight regarding relative differential binding properties of different AA ligands. Using the SigmaPlot software suite, the equation below for binding models was applied.

FIGURE 2: SigmaPlot Binding Model

$$\mathrm{F} = \mathrm{F}_{\mathrm{free}} - (\mathrm{F}_{\mathrm{free}} - \mathrm{F}_{\mathrm{bound}}) * \left(\frac{(\mathrm{Pt} + \mathrm{Lt} + \mathrm{KD}) - \sqrt{(-(Pt + Lt + KD))^2 - 4P_tL_t}}{2} \right) / Pt$$

LEGEND: *F represents the fluorescence signal that was observed at each ligand concentration (Lt) and Pt represents the total protein concentration. The amount of binding sites and respective affiniteies were determined for AA-I/AA-II interactions with HSA through application of isothermal titration calorimetry.*

Isothermal Titration Calorimetry (ITC)

The binding parameters for association of defatted HSAA3782 with AA-I and AA-II were obtained through calorimetrically employing a MicroCal VP-ITC instrument. The stock protein stolutions (which were 0.5mM to 1.5mM) were prepped by BME reduction in order to disrupt potential CyS34-CyS34 dimers and then dialyzed against three exchanges of 10mM sodium phosphate buffer (with a pH of 7.5). Portions of the AA ligand stocks were dissolved in protein dialysate with the final DMSO solution concentration moved to 2%. The HSA standards were prepped by diluting an appropriate portion in dialysate with 2% DMSO in order to match the solution contents in the syringe. All of the ITC experiments consist of 30 consecutive injections during which reaction heat was monitored and integrated across a 5 minute interval while being constantly stirred. The protocol enbsures that there was at least as 15-fold excess of either AA-I or AA-II (at 75um to 200uM) in the titration syringe in comparison to the starting HSA concentration (of 5uM to 10uM) in the reaction cell. Binding the isotherms obtained at 25C were created by recording the integrated reaction heats normalized for the AA concentration compared to ligand:protein ratio. In the ORIGIN software, analysis of the AA-HSA isotherms used single, tow-site, and sequential binding models showed inferior fits as a consequence of the difficulties faced in baseline assignments. They used the NITPIC/SEDPHAT/GUSSI suite of software programs in order to make sure the unbiased baseline assignments and the peak integrations that facilitated selection of appropriate binding models to characterize the protein-ligand systems. Non-linear least squares analysis of the resulting profiles invoking symmetrical two-site binding models provides optimal fit of the isotherms as well as requisite macroscopic parameters for the AA-HSA interactions.

X-Ray Crystallography

A novel method using HSAA3782 was used to prep monomeric HSA enriched with HSAMYR (myristic acid) for all of the crystallization studies. To obtain the monomeric HSA involved in dissolving lyophilized protein (at a concentration of 620uM) in 20mM KPi (with a pH of 7.5; buffer A). This sample was reduced in the presence of BME (at a concentration of 35mM) for small-scale preparations. The reducing agent was taken and concentrated HSA was produced by dividing the protein sample across six Amicon Ultra-15 centrifugal filter units and followed by spinning in a centrifuge at 4000g and 4C for 30 minutes. After the first spin in the centrifuge, the eluent was removed and discarded and the sample volume above the membrane was reduced to 1.5mL. Buffer A was added, followed by an additional spin in the centrifuge. This was repeated twice. As a whole, three buffer exchanges were made providing six protein solutions. The samples were combined and adjusted to a complete volume of 15mL in buffer A.

The resulting HSA stock (of 110mg/mL) is made up of at least 99.8% monomeric protein which is estimated by UV spectrophotometry and an Ellman's assay. The stock HSA was stored in -80C prior to crystallization or preps of complexes with sodium myristate. 2.63mM sodium myristate solution was prepped in buffer A (and stored at 4C until use) and then heated in a water bath at 50C to let dispersion of the fatty acid right before prep of HSAMYR. The myristate solution was cool quickly and added to monmeric HSAA3782, producing a 12:1 HSA (fatty acid) to myristate (protein) ratio. This sample was incubated for 1 hour at room temperature, occasionally mixing gently. The excess undissolved myristate was then pelleted through two spins in a centrifuge at 12000g and 4C for 5 minutes eacg spin. The remaining sample was divided into six filter units and then followed by spinning in a centrifuge and three successive exchanges of buffer using 0.1mM sodium myristate in buffer A. This produced 2875uM HSA enriched with HSAMYR which was then stored at -80C before crystallization.

Before cystallization the HSAMYR concentration was adjusted to 140mg/mL in buffer A with 0.1mM sodium myristate. The AA-I was suspended in buffer A in order to gain a maximal (w/v) concentration of 27mM. This HSAMYR/AA-I mix was prepped by mixing HSAMYR (at 2.1mM) and AA-I suspension, producing 2.7mM AA-I and 1.9mM HSAMYR in a 1.4:1 AA-I to HSA molar ratio. The HSAMYR/AA-II solution was created in a comparable method by mixing HSAMYR and 26mM AA-II that resulted in 5.2mM AA-II and 1.68mM HSAMYR in a 3:1 AA-II to HSA molar ratio. It was then incubated at 25C for 24 hours and the HSAMYR/AA-II suspensions were then spun in a centrifuge to remove and discard the undissolved AA-I/II and sodium myristate. The HSAMYR, HSAMYR/AA-I, and HSAMYR/AA-II solutions were prepped for cystallization using a hang-drop method. The HSAMYR, HSAMYR/AA-I, and HSAMYR/AA-II crystals grew from a condition having 28% to 30% polyethylene glycol (PEG) 3350 as well as 25mM sodium phosphate (with a pH of 7). Regarding the HSAMYRAA-I and HSAMYRAA-II complexes, crystallization drops had been prepped by mixing crystallization solution with a corresponding HSAMYR/AA mix and let to equiliberate over a reservoir at 25C for 24 hours. After equilibration, drops were streak-seeded using a 1:10^3 solution prepped with a SeedBead kit from Hampton Research from HSAMYR crystals that were grown similarly under conditions for crysallization containing 31% PEG 3350 as well as 50mM sodium phosphate (at pH 7). The crystals that formed were cryo-protected with brief soaking in reservoir solution and supplemented by 10% ethylene glycol.

Because AL-I-NOSO3 has a limited t1/2 when in aqueous solutions, they used the protective effect that HSA binding provides to gain HSA-metabolite co-crystallization complexes. AL-I-NOH and AL-I-NOSO3 stock solutions were dissolved in DMSO at 52mM and 55mM concentrations. Portions of the stock solutions were quickly added to HSADEFATTED at a 3-fold to 5-fold excess with the limit that the toal concentrations of DMSO that didn't pass above 15%. HSADEFATTED/AL-I-NOH and HSA/DEFATTED/AL-I-NOSO3 solutions were incubated overnight and were washed several times with buffer A using an Amicon centrifugal filter device having a 10kD cutoff. These solutions were then used for crystallization of HSADEFATTED/AL-I-NOH and HSADEFATTED/AL-I-NOSO3 under the same conditions for defatted HSA. Both HSA complexes provided optimal crystals via vapor diffusion with 33% PEG 3350, 25mM sodium phosphate, as well as a 1:1 complex/reservoir solution ratio. The drops were streak-seeded in 24 hours using stock unligated HSADEFATTED crystal seed. Post seeding, crystals grew to their maximal size after 7 days and started growing after 2-3 days. The complexes of HSAMYR/AL-I-NOH and HSAMYR/AL-I-NOSO3 were prepped analogously using myristate-

supplemented buffer A in the washing step. The crystals, regardless of quality were subject to x-ray synchrotron radiation and their structures determined at a low resolution.

Results

HSA Protect N-sulfonyloxyaristolactam From Decomposition and Extends the Reactivity with DNA

The initial study assessed if the presence of HSA affects the half-life of AL-I-NOSO3 in solution via monitoring the impact BSA has on its stability as a function of time in minutes. The AL-I-NOSO3 was incubated in the absence and in the presence of 600uM BSA across time periods from minutes to days. At prescribed time intervals, they combined sample portions with ice-cold methanol in order to make the BSA precipitate. With analysis through ESI-LC/MS (electrospray ionization liquid chromatography mass spectromery) made comparison of the free AL-I-NOSO3 in the supernatant relative to the amount at zero time, as seen in figure 3 below.

FIGURE 3: The ESI-LC/MS Stability in the Absence and Presence of BSA

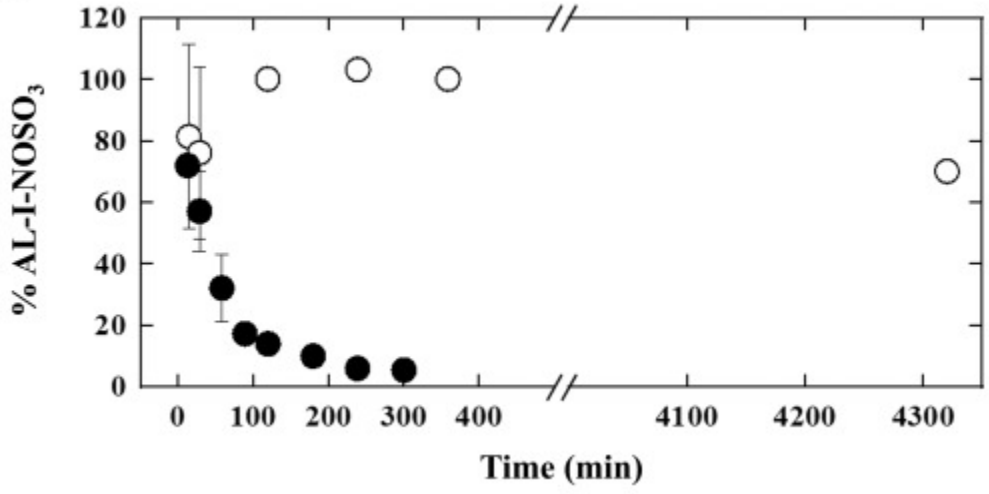

LEGEND: *The impact of HSA on the stability and activity of AL-I-NOSO3. The ESI-LC/MS stability of AL-I-NOSO3 in the absence of BSA is depicted with closed circles and in the presence of BSA is depicted with open circles. The AL-I-NOSO3 was incubated at various time intervals and followed by precipitation of protein and evaluation of the compound stability by mass spectrometry.*

The study was extended to study the impact of HSA on the metabolite activity. AL-I-NOSO3 was found to form less AL-DNA adducts when in the presence of HSA as a direct result of drug binding. Additionally, the AL-I-NOSO3 activity is not expected to degrade massively when incubated with HSA over several different time periods before the addition of DNA. The AL-I-NOSO3 incubated sans protein is expected to have a rapid decline in the reactivity of DNA over time. The results in figures 4, 5C, and 5D as seen below, support this.

FIGURE 4: The SDS PAGE of Reaction Mixtures Visualizing Al-DNA in the Absence and Presence of HSA

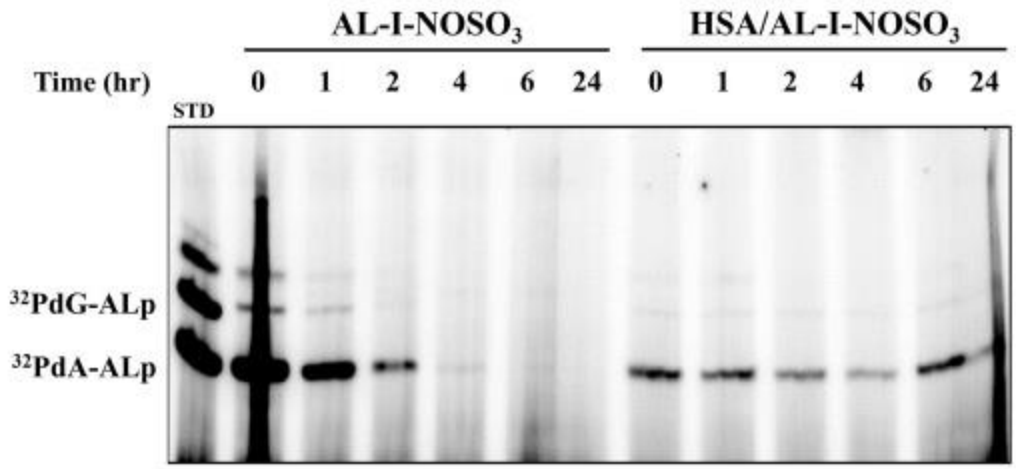

LEGEND: *The impact of HSA on the stability and activity of AL-I-NOSO3. The SDS PAGE of the reaction mixes involve 32P-postlabelling technique in order to visualize the AL-DNA in the absence (LEFT) and presence (RIGHT) of HSA for several time periods of time before the addition of DNA. The first lane depicts a mix (of 30 fmol each) of dA-AL-II and dG-AL-II oligonucleotides. The fragments above the 32PdG-AL-phosphate relates to digestion and labelling artifacts leftover that can sometimes be seen in certain batches of phosphodiesterases and kinases.*

FIGURE 5C/5D: The Gel Analysis and Quantification in the Absence and Presence of HSA

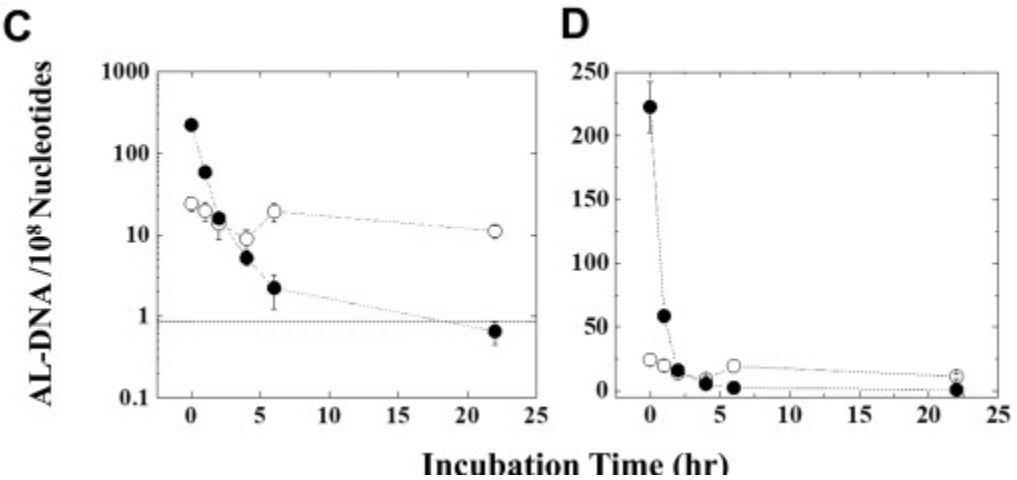

LEGEND: *The impact of HSA on the stability and activity of AL-I-NOSO3. The gel analysis and quantification in the presence of HSA is depicted by open circles and the absence of HSA is depicted by closed cirlce. This is shown in logarithmic and linear scales. The AL-DNA levels depict the sum of all fragments detected in the gel. Additionally, each data point shows the mean and the standard deviation gained from 3-6 DNA reactions. The dashed line represents the minimal level of detection.*

When diluting the AL-I-NOSO3 in phosphate buffer (at the zero time point), the AA metabolite forms 225 AL-DNA adducts per 10^8 nrcleosides after incubation for 30 minutes with DNA. In similar conditions, a AL-I-NOSO3 solution pre-incubated when in the presence of HSA shows ten times less reactivity when exposed to DNA. This results in the creation of 25 AL-DNA adducts per 10^8 nucleosides. When the AL-I-NOSO3 is let to incubate in buffer alone for several different time periods

before the DNA addition, the activity declines 10-fold within a 2 hour time period, decreasing to the level detected between 6 hours and 24 hours. Surprisingly, for 24 hours, the AL-I-NOSO3/HSA activity mix remained somewhat constantly fluctuating near the zero time point level. The adduct formation in presence of HSA relates to ~10% of the AL-I-NOSO3 sans albumin (the control), which suggests that ~90% of the metabolite stays sequestered in equilibrium conditions. As a whole, these results show that AL-I-NOSO3 binding to HSA protects the AA-I sulfonated metabolite from decomposing and prevents DNA addcut forming in vitro.

The HSA Fluorescnece Quenching Assays

The ligand-induced quenching of intrinsic HSA was assessed by observing and watching a single Trp214 residue that is located within the IIA binding cavity in order to obtain equilibrium dissociation constants (KD) for several exogenous molecules and endogenous molecules, including aristolochic acids. Studies usually focus on the commercial preps of HSA that don't specify the fatty acid content, the amount of CyS34-CyS34 protein dimers, as well as the ratio of modified CySH34 in the samples. In acknowledgement of this deficiency, meracaptoalbumins from HSAA3782 and HSAA8763 were prepped, consisting of limited fatty acid-containing HSA and fatty acid-free containing HSA. The study used the well-defined HSA samples in order to make comparative fluorescence quenching studies when in the presence of AA-I/AA-II as well as their metabolites while at the same time evaluating impacts of fatty acid content on the relative binding affinites. Fluorescence quenching profiles can be seen in figure 6 and 7 below and the resulting data is summerized in table 1 below.

FIGURE 6: The HSA-AA Binding Profiles Found Through Fluorescence Quenching Assays of Trp214

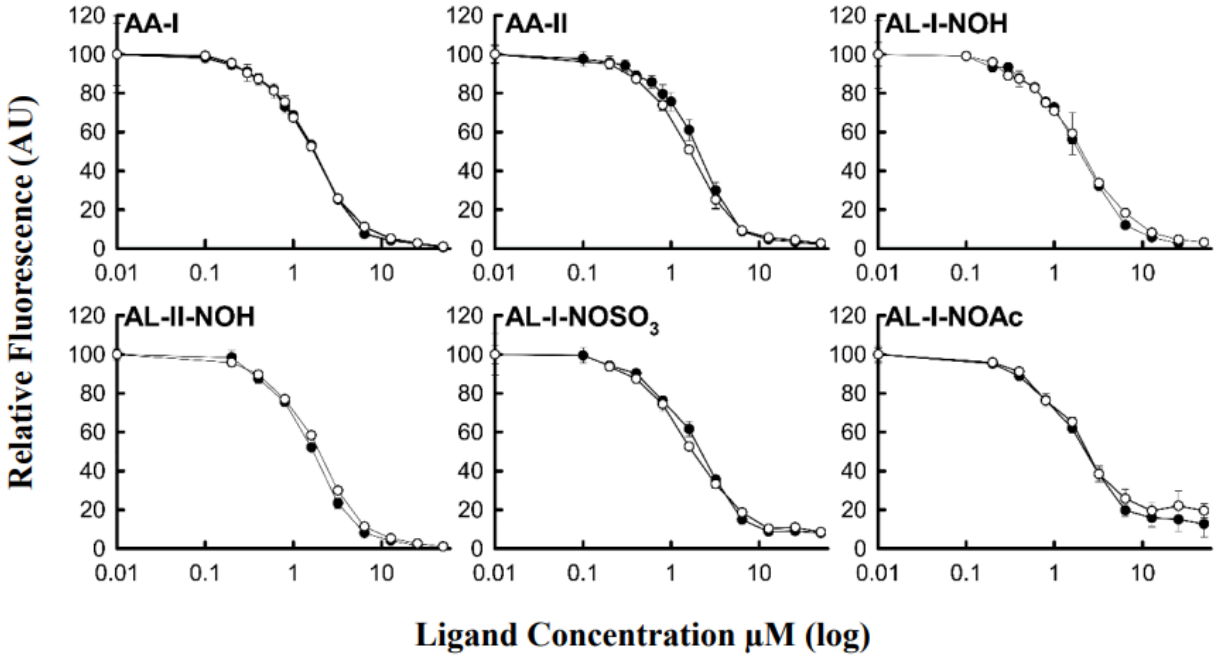

LEGEND: *The HSAA3782 is represented by closed circles and the HSAA8763 is represented by open circles, were incubated in the presence of AA-I, AA-II, AL-I-NOH, AL-II-NOH, AL-I-NOSO3, and AL-I-*

NOAc. Intrinsic Trp214 fluorescence intensity (lamdaEX = 295nm; lambdaEM = 340nm) was recorded for the HSA/AA ratios to make the relating ligand-induced quenching profile. Maximum fluorescence intensity seen for HSA in absence of AA species were assigned as reference and each data point shows the mean and standard deviation of equilibrium titration for 3-5 independent experiments.

FIGURE 7: The Dissociation Constants (KDapp) for AA and Metabolite Complexes in the Presence (HSAA8763) and Absence (HSAA3782) of Fatty Acids

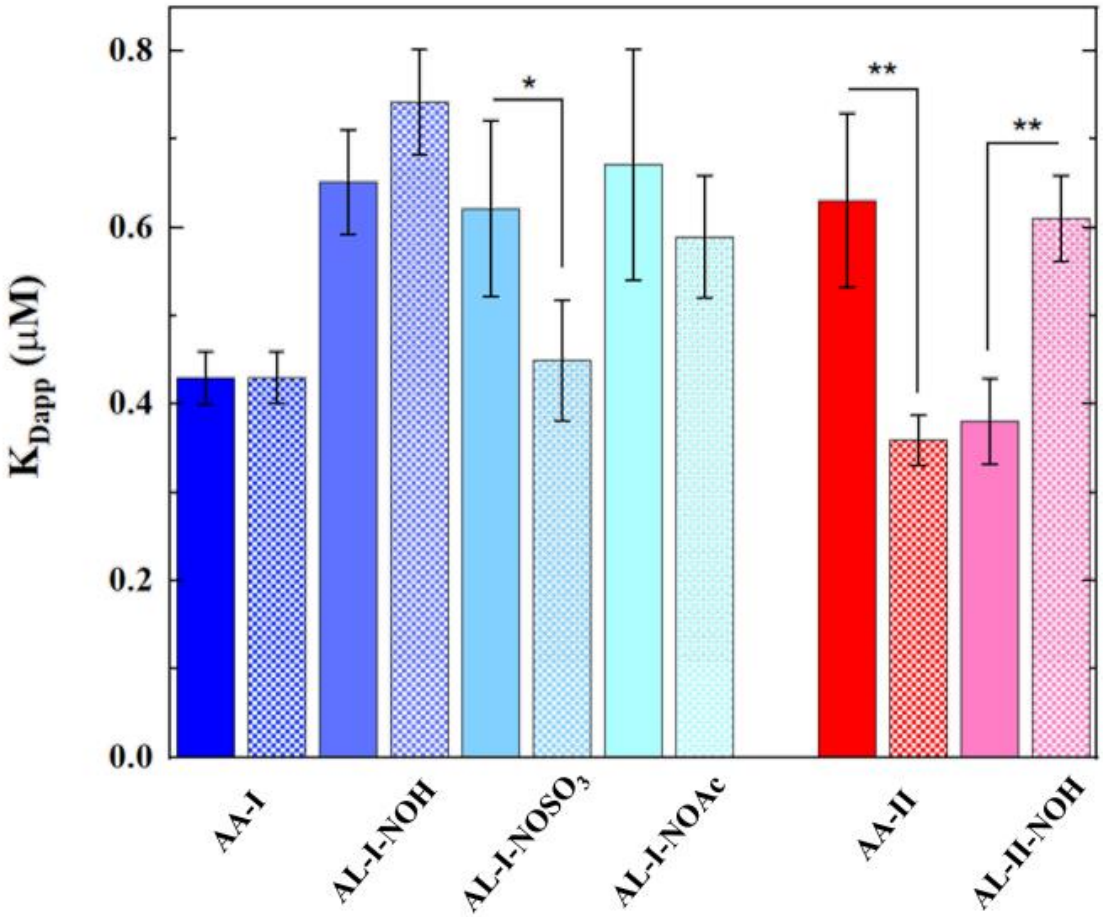

LEGEND: *This data is reported at the mean +/- SD with statistical importances found through One-Way ANOVA and Turkey Tests using confidence levels of p<0.05(**) and p<0.10(*). The differences in KDapp were calculated for AA ligand interactions with fat-free (HSAA3782, solid) in comparison to fat-containing (HSAA8763, checkerboard) protein preps.*

TABLE 1: The Dissociation Constants (KDapp) From Fluorescence Quenching Assays of HSA via Aristolochic Acids and Metabolites

Ligand	$K_{D_{app}}$ (HSA_{A3782})	$K_{D_{app}}$ (HSA_{A8763})
AA-I	**0.43 ± 0.03**	**0.43 ± 0.03**
AL-I-NOH	0.65 ± 0.06 **	0.74 ± 0.06 **
AL-I-NOSO3	0.62 ± 0.10 *	0.45 ± 0.07
AL-I-NOAc	0.67 ± 0.13 **	0.59 ± 0.07
AA-II	**0.63 ± 0.10**	**0.36 ± 0.03**
AA-II-NOH	0.38 ± 0.05 **	0.61 ± 0.05 **

LEGEND: *The apparent dissociation constants (KDapp) are shown as the mean +/- SD for 3-5 independent measurements of the AA species in the presence (HSAA8763) as well as absence (HSAA3782) of fatty acids. The binding data was evaluated through One-Way ANOVA and Turkey Tests using confidence levels of p<0.05(**) and p<0.10(*) to find any statistically important differences for KDapp for every metabolite corresponding to the unmodified AA-I/AA-II ligand.*

Figure 6 shows the observed differential impacts of fatty acids on HSA interactions with AAs and the active metabolites were compared by the quenching profiles of HSAA8763 and HSAA3782 when in the presence of AA-I, AA-II, AL-I-NOH, AL-II-NOH, AL-I-NOSO3, and AL-I-NOAc. Table 1 summarizes that relative to unmodified AA-I, the correlating metabolites with an exception of AL-I-NOH, exhibits an increased KDapp that is effectively repelled when in the presence of fatty acids. Suprisingly, the KDapp seen in AA-II binding to defatted protein is more than that of AA-I, however, greatly decreased when in the presence of fatty acids. Alternatively, the AA-II-NOH metabolite shows a better binding affinity to HSA when in the presence of fatty acids. As seen in figure 7, the presence of fatty acids consequently differentially impacts ligand-dependent HSA quenching by increasing (the AL-II-NOH) or by decreasing (the AL-I-NOSO3 and/or AA-II) the dissociation constant. These discoveries may reflect binding to specific sites within HSA and/or varying degrees of independence betwixt the fatty acid interactions and ligand interactions. Because HSA quenching profiles of Trp214 produce concentration-dependent KDs and the latter prevents accurate determination of the binding parameters under the conditions of this study. As a result, characterization of AA-HSA affinity constants and the stoichiometry needs the employment of different approaches that don't rely on the intrinsic fluorescent probes.

The Characterization of AA-HSA Interactions by ITC

The binding affinities of AA-I and AA-II for HSAA3782 were evaluated by conducting a series of ITC experiments in this study. The obtained binding isotherms at different AA(100-200uM) and HSA(5-10uM) concentrations made optimization of solution conditions easier by minimizing unnecessary species as well as making sure that ligand aggregation and/or precipitation doesn't appreciably impact the resulting calorimetric profiles. The initial evaluation of AA-HSA binding isotherms using conventional programs for fitting give an estimate for the binding stoichiometry of two AA ligands per each HSA molecule. The analysis of ITC profiles shows the formation of the AA-HSA complex is exothermic and

can be characterized by micromolar binding affinities. The NITPIC/SEDPHAT/GUSSI software suite was used to make sure unambiguous evaluation of the binding isotherms. The singular value decomposition produces baseline-corrected association data that get analyzed through a two-site binding model in order to obtain macroscopic affinities for AA-HSA interactions. The equation in figure 8, below, is in accordance to the interactions.

FIGURE 8: Equation for AA-HSA Interactions

$$A + B + B \leftrightarrow [AB] + B \leftrightarrow ABB$$

LEGEND: *A depicts the HSA macromolecule and B depicts ligand AA-I or AA-II. This model for binding suggests that both sites are involved with all possible states of ligation coexisting in equilibrium.*
It was determined that macroscopic affinity constants for a family of binding isotherms obtained at 25C, as seen in figure 9, below.

FIGURE 9: The Characterization of AA-HSA Binding Energetics by ITC

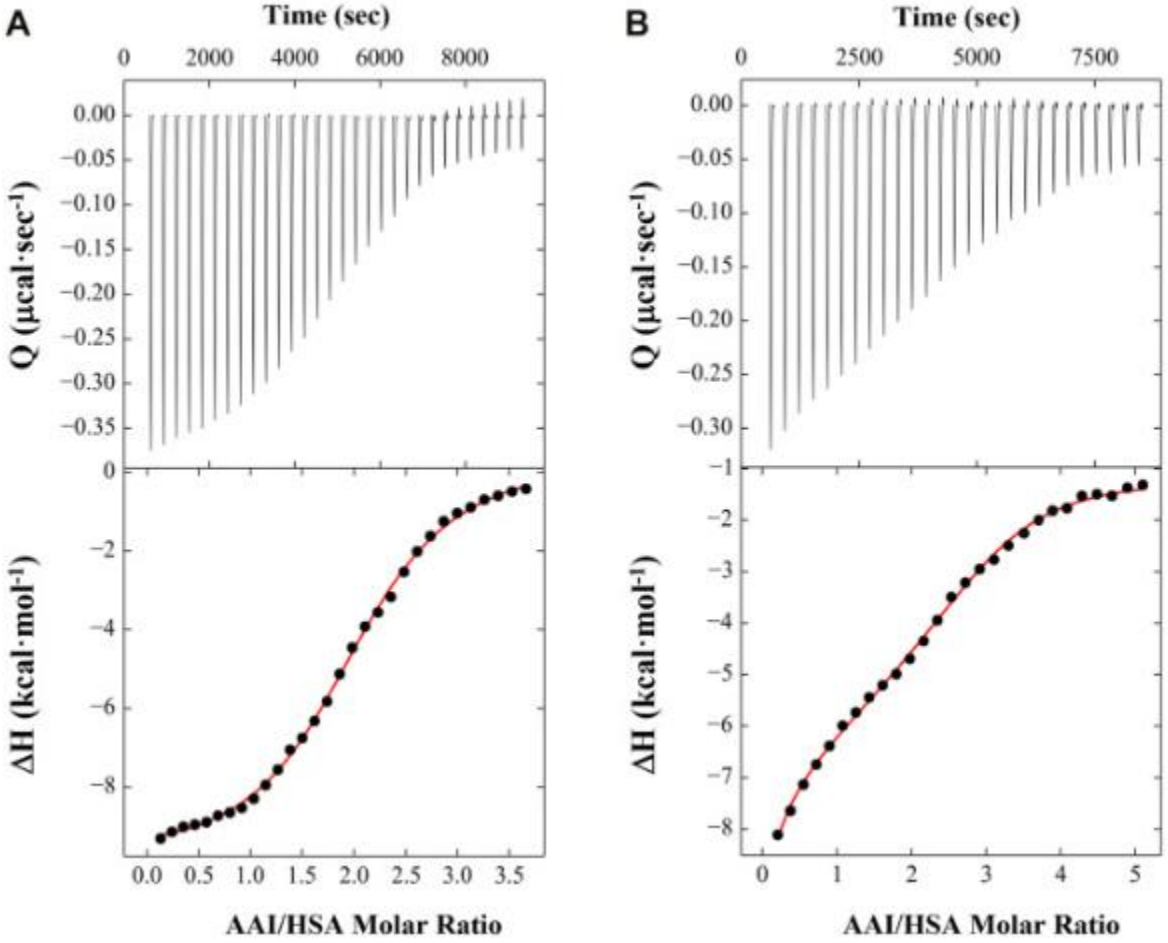

LEGEND: *The characterization of AA-HSA binding energetics by ITC. The representative ITC profiles for the association of AA-I (A) and AA-II (B) with HSA. The lower panals show integrated binding*

isotherms, represented by black circles, expressed as a function of the AA:HSA ratios. The upper panels relate to exothermic reaction heats created by the titration of AAs into HSA. The data resulting is fit to a model of two binding sites, represented by the red lines, in order to produce the macroscopic association constants seen in table 2.

Formation of AA-HSA complexes are defined by moderate binding affinities from 10^5 to 10^6M^-1. Evaluation of calorimeteric profiles and resulting parameters show both AA ligands show two-site binding modes having macroscopic affinity constants (Ka) of 1.5*10^6M^-1 and 5.4*10^5M^-1 for AA-I in comparison to 8.4*10^5M^-1 and 9*10^5M^-1 for AA-II, as sumarized in table 2, below. The correlating KD are 0.69 and 1.87uM for AA-I in comparison to 1.19 and 1.11uM for AA-II. Analysis using a two-site binding model shows that the AA-HSA interactions that entail two distinct sites that may show independent or mutual events. This result is consistent with unique HSA multisite binding properties.

TABLE 2: The Binding Parameters Produced for the Association of AA-I and AA-II with HSA

Ligand	Binding site	$K_a \cdot 10^6$ (M^{-1})	K_D (μM)	ΔG° (kcal·mol^{-1})
AA-I	Site 1	1.50 ± 0.18	0.69 ± 0.08	−8.41 ± 1.00
	Site 2	0.54 ± 0.04	1.87 ± 0.12	−7.82 ± 0.58
AA-II	Site 1	0.84 ± 0.07	1.19 ± 0.19	−8.10 ± 0.67
	Site 2	0.90 ± 0.10	1.11 ± 0.11	−8.12 ± 0.82

LEGEND: *The binding parameters produced for the association of AA-I and AA-II with HSA. The binding afffinities are produced from non-linear fits of the ITC profiles, as seen in figure 9, to a model that is comprised of two sites that produce the required macroscopic association constants. The binding data relating to average values as well as standard deviations determined for a minimum of 3 ITC measurements carried out in 10mM NaPO4 (at pH 7.5) at 25C. The resulting binding free energies are calculated by the standard thermodynamic relation: delta G = -RTlnKa (with T = 298K).*

The Structural Analysis of HSAMYR and HSAMYR/AA Complexes

Before trying to fing specific binding interactions between HSA and AA species, the crystallization and determination of molecular structue of HSA in presence and absence of AA-I/AA-II. Monomeric HSA species enriched with sodium myristate was prepped to gain high-quality HSA crystals. This made the determination of the structure of HSAMYR and its complexes with AA-I/AA-II possible at 1.9A resolution. Crystal structures gained under the conditions of this experiment were affected by the presence of strong tNCS (translational non-crystallographic symmetry). Surprisingly, the presence of tNCS didn't complicate the molecular replacement because of the availability of HSA models but could account at

least in part for elevated R-factor statistics. The refinement parameters of HSAMYR, HSAMYR/AA-I, and HSAMYR/AA-II and their accession numbers can be seen in table 3, below, and the individual B-factors and relating ligand occupancies can be seen summarized in table 4, below.

TABLE 3: Represents Data Collection and Refinement Parameters for Crystal Structures

Protein	HSA_{MYR} complex	HSA_{MYR}/AA-I complex	HSA_{MYR}/AA-I complex (2 AA-I)	HSA_{MYR}/AAII complex
Data Collection and Refinement				
Beamline	DIAMOND-i03	ESRF-BM30	ESRF-BM30	DESY-P13
Processing software	DIALS	XDS	XDSGUI	DIALS
Space group	$P12_11$	$P12_11$	$P12_11$	$P12_11$
Wavelength (Å)	0.9762	0.9798	0.9798	0.9786
Rotation range (°)	293	227	227	259
Oscillation range Δφ (°)	0.1	1	1	0.1
Unit cell dimensions (Å)				
a	95.728	94.397	95.247	94.821
b	38.562	37.872	38.189	38.671
c	183.557	180.248	181.918	180.841
Resolution (Å)	88.79–1.90 (1.93–1.9) [a]	45.56–1.9 (1.968–1.9)	45.98–1.93 (1.93–1.90)	174.74–1.9 (1.93–1.9)
No. of reflections				
Total	523,824 (19,220)	411,167 (36,809)	409,672 (15,687)	464,097 (22,161)
Unique	102,879 (4432)	97,365 (9562)	99,387 (4618)	101,166 (4813)

Multiplicity	5.1 (4.3)	4.2 (3.8)	4.1 (3.4)	4.6 (4.6)
Completeness (%)	98.7 (85.6)	98.8 (98.65)	98.5 (95.0)	99.3 (95.4)
<I/σ(I)>	7.5 (0.7)	10.93 (2.53)	10.9 (2.7)	6 (0.9)
Wilson B-factor	31.7	26.35	23.85	32.63
R_{meas} (%)	0.095 (1.341)	0.08848 (0.5427)	0.087 (0.542)	0.090 (1.371)
R_{pim} (%)	0.042 (0.616)	0.04216 (0.2654)	0.041 (0.275)	0.041 (0.618)
CC half	0.996 (0.599)	0.996 (0.796)	0.997 (0.802)	0.995 (0.633)
R_{work} (%)	0.2243 (0.3857)	0.2402 (0.3421)	0.2305 (0.3231)	0.2304 (0.3371)
(no. of reflections)	102,482 (9781)	97,330 (9557)	99,346 (9497)	99,375 (9864)
R_{free} (%)	0.2687 (0.4471)	0.2894 (0.3600)	0.2807 (0.3686)	0.2710 (0.3708)
(no. of reflections)	5037 (449)	4931 (492)	5016 (480)	4715 (467)
Refined Model				
No. of protein chains	2	2	2	2
No. of residues	1164	1164	1164	1164
No. of ligands atoms	724	685	610	680
No. of solvent molecules	659	529	544	594

No. of atoms (overall) (non-H)	10,100	9969	9974	10,055
<B> factor (Å^2) overall	40.19	41.35	41.72	43.86
<B> factor (Å^2)				
Macromolecules	39.78	41.53	41.96	43.55
Ligands	45.44	41.78	43.63	45.50
FA	51.07	49.54	50.52	51.62
AA	--	26.07	46.60	43.08
Solvent	43.83	38.11	36.86	47.77
Mean ligand occupancy				
FA	0.93	0.93	0.92	0.88
AA		0.88	0.92	0.89
Ramachandran plot				
Favored (%)	98.36	97.50	98.02	98.10
Allowed (%)	1.64	2.50	1.98	1.90
Disallowed (%)	0.00	00.20	0.00	0.00
RMS deviation				
Bond lengths (Å)	0.010	0.004	0.008	0.004
Bond angles (°)	1.10	0.66	0.90	0.57
PDB code	8RCP	8RGK	8RGL	8RCO

LEGEND: *Values for the highest-res shell are in parentheses.*

TABLE 4: The Ligand Occupancies and B-Factors

	HSA-Myr (8RCP)				HSA-AA-I (8RGK)				HSA-AAI (Two Copies) 8RGL				HSA-AA-II (8RCO)				All Structures	
	Chain A		Chain B		Chain A		Chain B		Chain A		Chain B		Chain A		Chain B			
Ligand	B-factor	Occupancy	B-factor	Occupancy	B-factor	Occupancy	B-factor	Occupancy	B-factor	Occupancy	B-factor	Occupancy	B-factor	Occupancy	B-factor	Occupancy	Average B-factor	Average Occupancy
FA1	51.34	0.92	49.00	0.87	65.94	1	--	--	--	--	--	--	48.38	0.79	49.41	0.81	52.81	0.88
FA2	53.33	1	50.72	0.97	54.63	0.92	30.13	0.97	29.03	0.9	62.25	0.95	52.58	0.92	49.97	0.85	47.83	0.94
FA3	44.48	0.94	51.61	0.96	50.25	0.89	32.93	0.83	26.69	0.84	48.58	0.86	52.84	1	48.02	1	44.42	0.92
FA4	54.50	0.91	56.11	0.93	54.15	0.78	42.91	1	42.26	0.98	54.90	0.85	55.41	0.87	56.20	0.87	52.05	0.90
FA5	53.24	1	55.24	0.98	65.21	0.93	51.46	1	53.21	0.96	71.15	1	56.14	0.9	59.48	0.9	58.14	0.96
FA6	45.00	0.92	47.17	0.92	55.80	0.77	36.51	0.96	53.21	0.96	62.04	0.79	46.35	0.87	44.69	0.78	48.85	0.87
FA7	51.61	0.95	50.87	0.92	64.82	1	39.27	1	34.94	0.93	68.02	1	--	--	--	--	51.59	0.97
FA10	49.92	0.82	53.06	0.83	--	--	--	--	--	--	--	--	--	--	--	--	51.49	0.83
AA-I Site IB	--	--	--	--	--	--	26.07	0.88	24.94	0.93	68.26	0.91	--	--	--	--	39.76	0.91
AA-II Site IIA	--	--	--	--	--	--	--	--	--	--	--	--	39.05	1	37.82	0.97	38.43	0.99
AA-II Site IB Lip	--	--	--	--	--	--	--	--	--	--	--	--	47.24	0.79	48.20	0.81	47.72	0.80
Per-Structure:	B-factor		Occupancy		B-factor		Occupancy		B-factor		Occupancy		B-factor		Occupancy			
Average FA	51.07		0.93		49.54		0.93		50.52		0.92		51.62		0.88			
Average AA					26.07		0.88		46.60		0.92		43.08		0.89			

LEGEND: *Compiled individual occupancies and B-factors of ligands present in the crystal structures. The per-chain fatty acid and aristolochic acid I/II averages are shown in the two bottom lines and the per-ligand averages show in the two rightmost columns.*

The HSAMYR structure has two protein molecules within the assymmetirc unit, which takes on a conformation that is similar to HSAMYR structures previously reported.

FIGURE 10: The Structure of the HSAMYR Complex

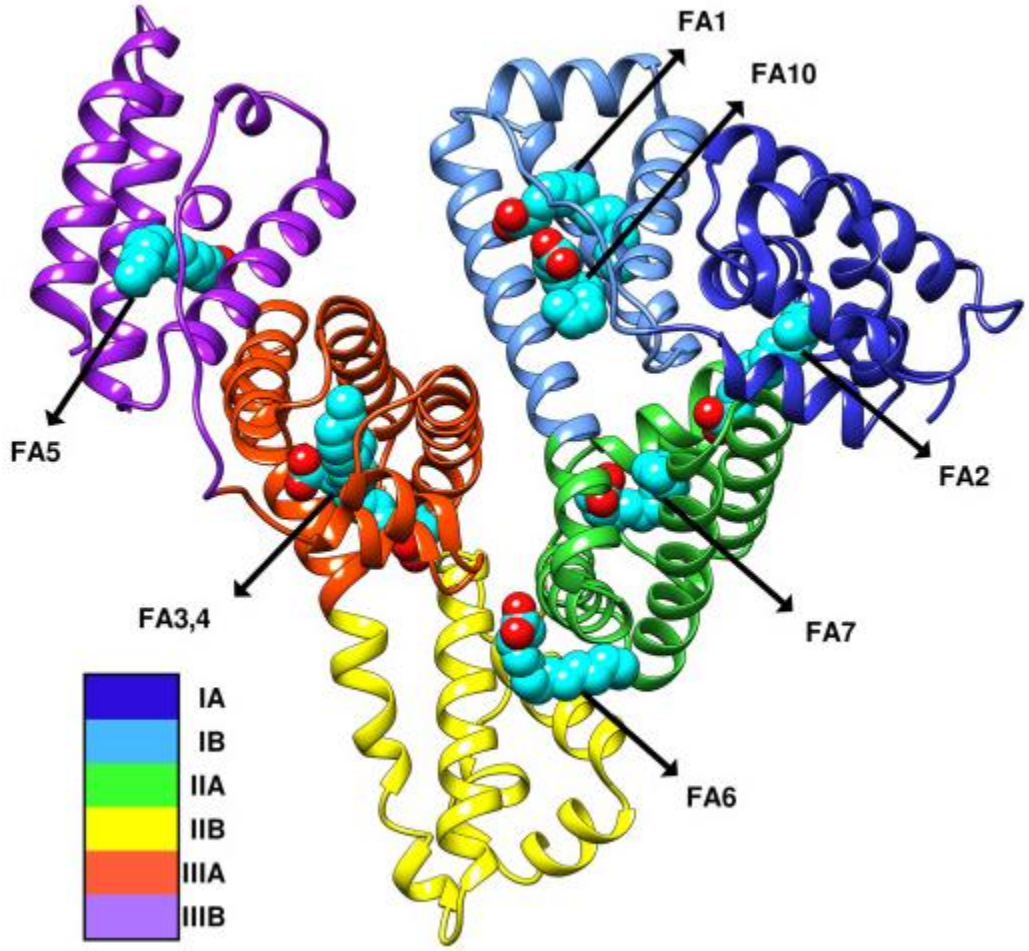

LEGEND: *The structure of the HSAMYR complex. A secondary ribbon structure is representation of the HSAMYR complex, colored by the individual subdomains. Fatty acid (FA) as well as drug binding sites are shown by the arrows with myristate ligands (light blue color). Many of the FA/drug binding sites are indicated by common designations: FA7 = drug site 1 = subdomain IIA; FA3,4 = drug site 2; FA1,10 = drug site 3 = subdomain IB.*

Under the crystallization conditions of this experiment, myristic acid ligands occupy known HSA primary fatty acid binding sites (FA1-7), as seen in figure 10. In comparison, the majority of existing HSAMYR structures reported, a second myristate molecule can be seen at the lip of subdomain IB as well as the classic FA site 1, located between Y161 and Y138. This implies that the presence of two distinct FA sites in the subdomain IB can be seen in figure 11, below.

FIGURE 11: The Structure of HSAMYR Subdomain IB Binding Site

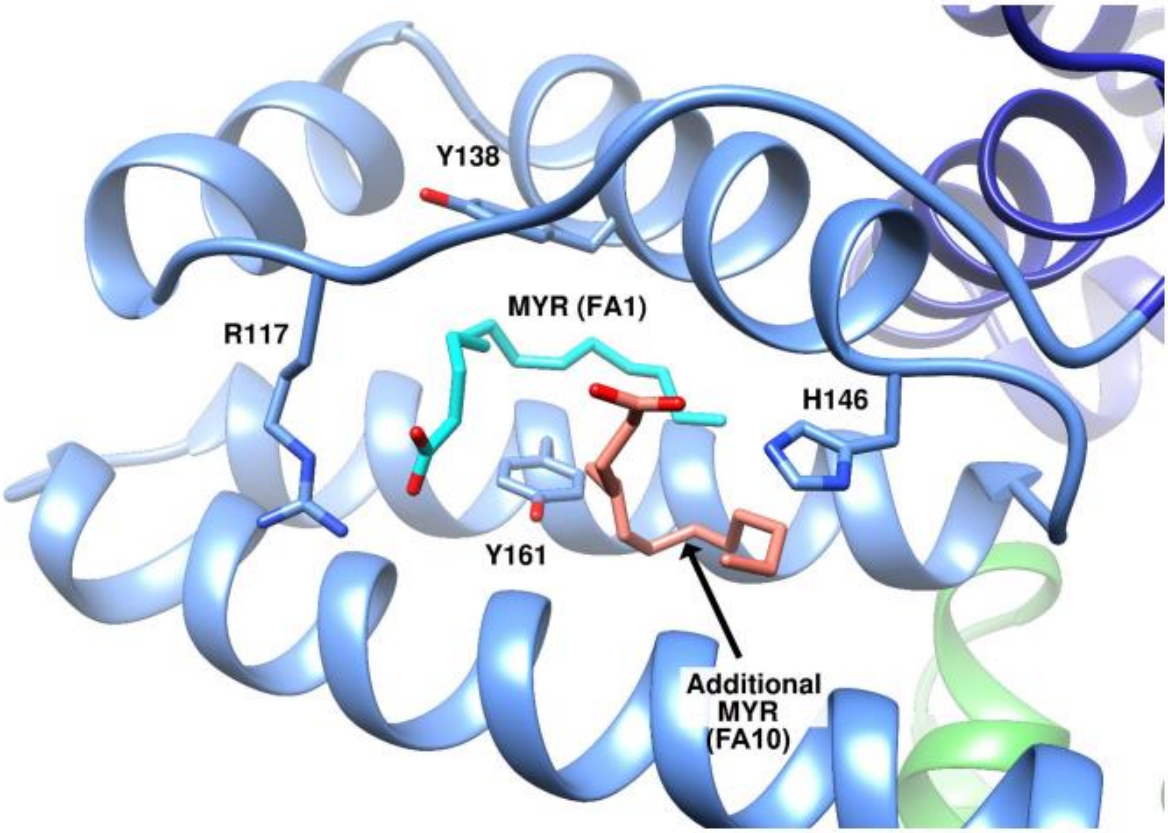

LEGEND: *The subdomain IB binding cleft takes on an "open" conformation and is occupied with two distinct myristate molecules.*

Binding of an extra myristate molecule is defined by a refined occupancy of 0.82-0.83, as seen in table 4. These values are slightly lower compared to the average occupancy in classical sites (0.94-0.95).

<u>The Structure of the HSAMYR/AA-I Complex</u>

The HSAMYR/AA-I structure shows that AA-I occupies the main space within the subdomain IB, replacing the myristate ligands (FA1, FA10) in HSAMYR as seen in image A of figure 12, below. The electron density of AA-I bound to one of the HSA chains is clear that the crystal structures, as seen in image B of figure 12, below, the second HSA has what looks like AA-I and myristate bound at mixed occupancy. The 2 structures of the HSAMYR/AA-I complex were modeled. A structure contains AA-I bound to subdomain IB of the HSA chain B and a myristate molecule in the position of HSA chain A, when another structure has AA-I modeled in subdomain IB binding space of every chain.

FIGURE 12: The Structure of HSAMYR/AA-I Complex

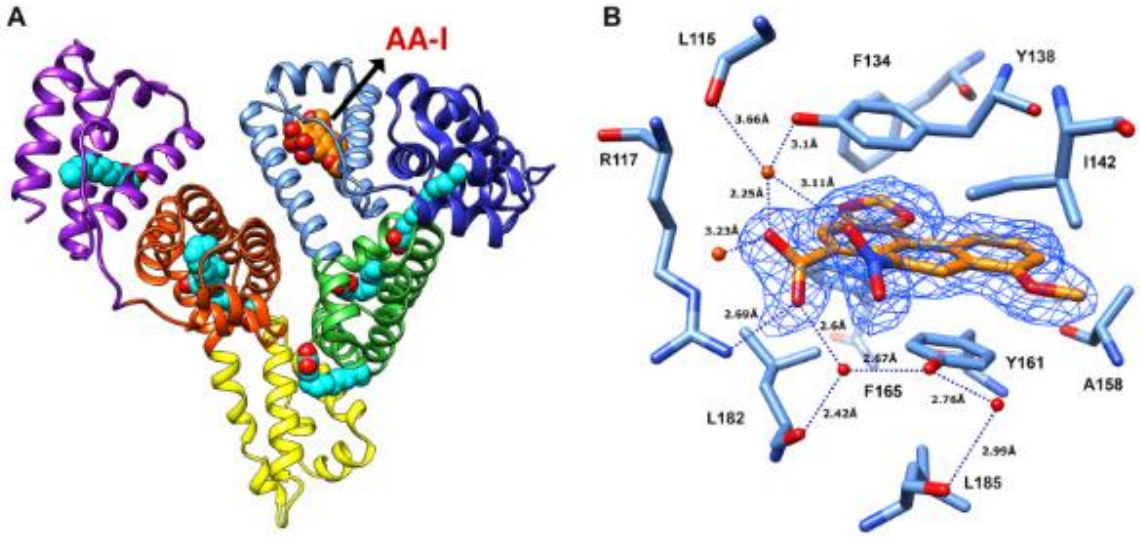

LEGEND: *Image A depicts the AA-I occupying the FA site 1 in subdomain IB. Image B depicts the residues and interactions that surround the AA-I bound in the space of subdomain IB (chain A). The 2Fo-Fc electron density of the AA-I is contoured at 1sigma (blue mesh) with hydrogen bonding distances (blue dotted lines), and adjacent water molecules and residues.*

In both cases, AA-I molecules are bound to subdomain IB in its open form, compared to that observed in HSA bound to myristate or hemin. In the bound state, AA-I is nealy totally buried in the binding space whereas only the carboxylate and nitro groups stick out slightly in the direction of the solvent, as seen in image A of figure 13, below. The electron density of AA-I is clear in showing its exact orientation/position within the binding site, as seen in both images of figure 13, below. The methylenedioxy ring of AA-I faces towards the F134 HSA residue and is lodged deep within the space. The methocy group of AA-I faces in the opposite direction and occupies the region of IB binding cleft, as seen in image B of figure 13, below. That region holds a portion of the bulky hemin ring in the previous HSA-hemin complex structures, as seen in image A of figure 14, below.

FIGURE 13: The Aristolochic Acid I Bound in HSA Subdomain IB Site

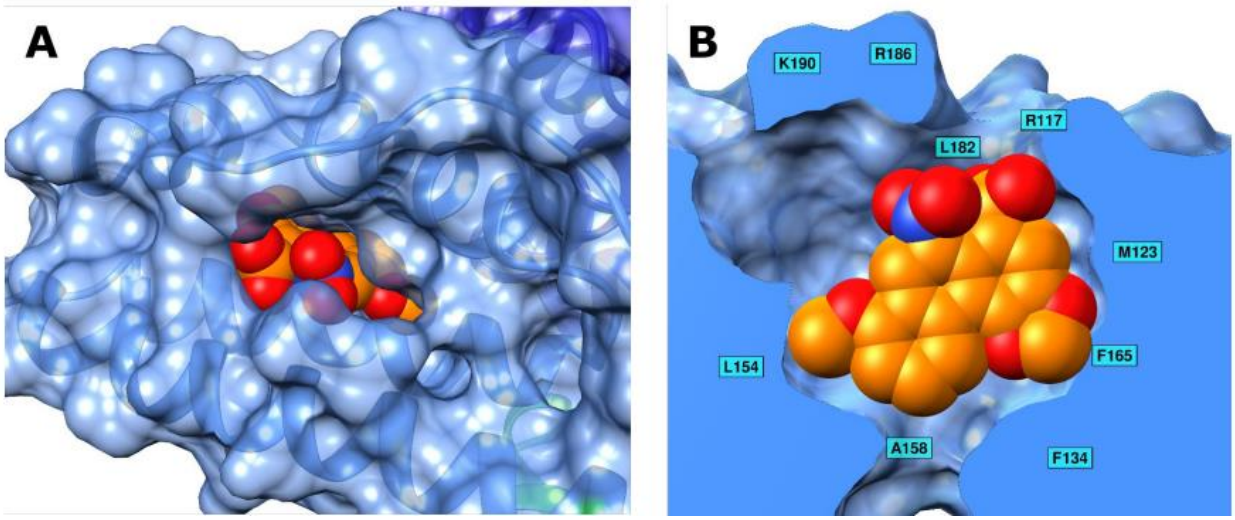

LEGEND: *Image A shows AA-I bound deeply in subdomain IB at its original location, FA1, with only the carboxylate and nitro groups sticking out towards the solution. Image B shows the shape of the subdomain IB binding space viewed through a cutaway of the HSA molecule surface. AA-I is bound near the inner side where it's surrounded by aromatic and aliphatic residues. The carboxylate and nitro groups aim towards a cluster of positively charged resides at the lip of the space.*

FIGURE 14: The Superimposition of AA-I (A) and AA-II (B) with Ligands that Bind to HSA Subdomains IB and IIA

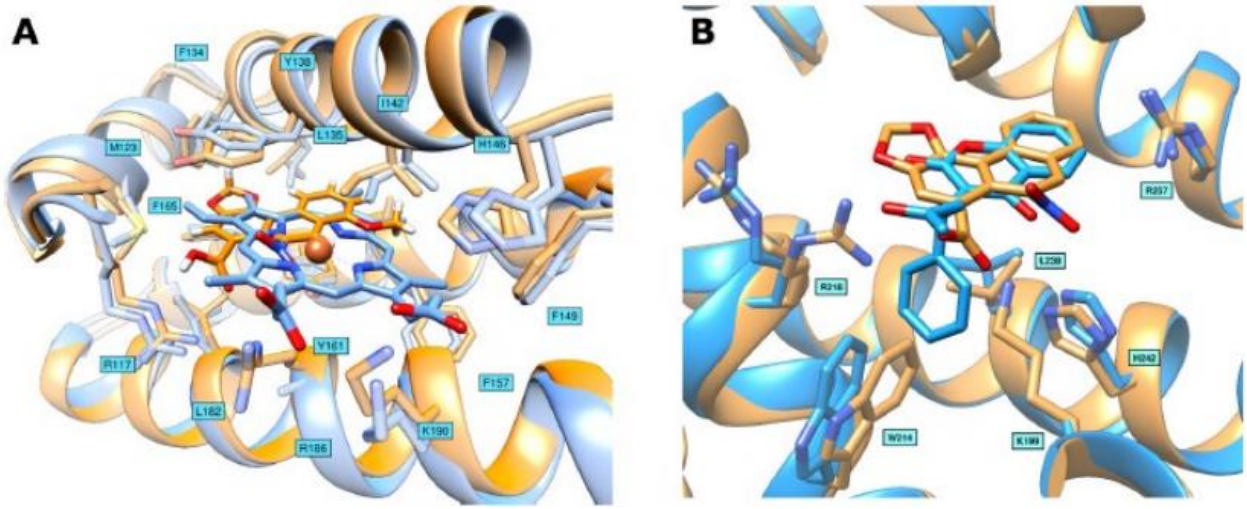

LEGEND: *Image A shows AA-I (orange) and hemin (light blue) that is bound in HSA subdomain IB (drug site 3). Both of the ligands bind deeply in the subdomain IB binding space as the planar portions are involved in hydrophobic and pi-stacking interactions while the complex can be stabilized by hudrpgen bonding as well as electrostatic interactions with residues at the opening of the site. Image B shows AA-II (orange) and warfarin R-(+) (blue) bound within the subdomain IIA (drug site 1). The cyclic moieties of both of the ligands occupy a similar plane in the subdomain IIA that orients their hydrophilic groups in an orientation that helps hydrogen bonding to basic residues at the opening of the binding site.*

The HSA residue R117 that is located at the opening of the space forms a hydrogen bond with carboxylate moiety of AA-I, as seen in figures 12 and image A of figure 15, below. The latter is h-bonded with Y138 via a bridging water molecule located at a distance from the nitro group of AA-I within chain A.

FIGURE 15: The Ligplot Diagrams Showing Binding Sites in HSA/AA-I (A) and HSA/AA-II (B/C)

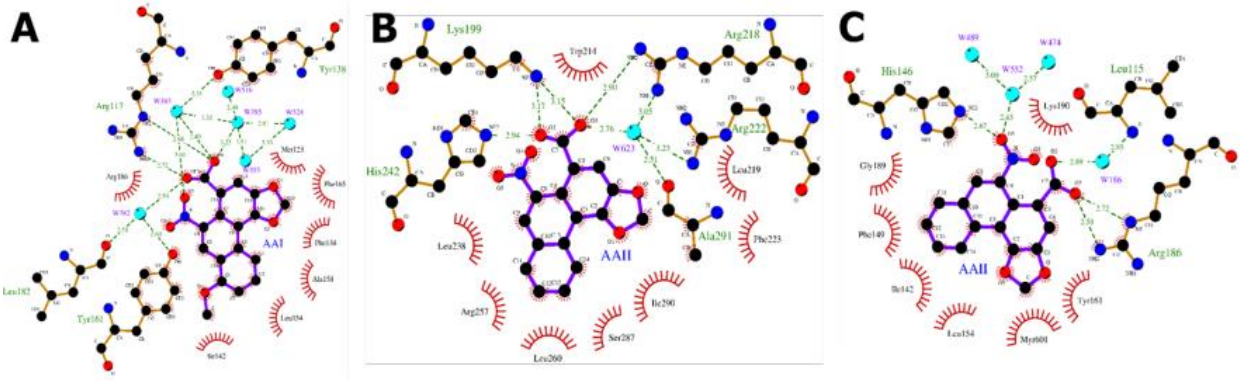

LEGEND: *Image A shows the interactions formed betwixt AA-I and residues of subdomain IB space in the HSAMYR/AA-I complex. Image B shows the interactions formed betwixt AA-II and residues of the subdomain IIA(drug site I) in the HSAMYR/AA-II complex. Image C shows the interactions formed by AA-II with the lip region of site IB in the HSAMYR/AA-II complex. The hydrogen bonds are shown with green dashed lines and hydrophobic contacts shown by red spokes.*

The carboxylate group in AA-I looks to be involved in an extra water bridge with Y161 as well as the main chain carbonyl of L182, as seen in image B in figure 12 and image A in figure 15. Tight h-bonding arrangement looks like that of the carboxylate moiety in FA1 bound to subdomain IB of HSAMYR. Surprisingly, R186 creates an h-bond with the nitro group of AA-I in a chain, however, this residue and K190 in the other chain points out to the solution and don't seem to create specific interactions involving the nitro group despite the close proximity. Those differences betwitx the two HSA chains may be connected, at least partially, to the mixed occupancy of AA-I in a chain. Apart from interactions created through the formation of the carboxylate and nitro groups with nearby HSA residues and water molecules, AA-I is snuggly bound by hydrophobic interactions with aromatic and aliphatic residues that coat the inner side of the space. Two of the HSA tyrosines in this area (Y138 and Y161 are spread out and AA-I occupies the space betwitx those residues, as seen in image B of figure 12. The AA-I is smushed between Y138 and Y161 in a parallel pi-stacking arrangement. The F134 and F165 that surrounds AA-I from the direction of a methylendioxy ring, whereas A158, I142, and F157 region AA-I on the methoxy group area, as seen in image A of figure 15. With the combination of snug h-bonding as well as hydrophobic interactions being consistent with strong binding and fixed arrangement of AA-I at the FA1 site. The results coupled with a high-refined occupancy of 0.91 are assumingly the result that the binding is seen in the HSAMYR/AA-I crystal structure.

<u>The Structure of the HSAMYR/AA-II Complex</u>

The high-res structure of the HSAMYR/AA-II complex can be seen in figure 16, below, shows two locations for the AA-II ligand, drug site 1 (subdomain IIA) and 3 (subdomain IB). The AA-II effectively moves FA7 and FA10 myristate molecules in drug sites 1 and 3, leaving FA1.

FIGURE 16: The Structure of HSAMYR/AA-II Complex

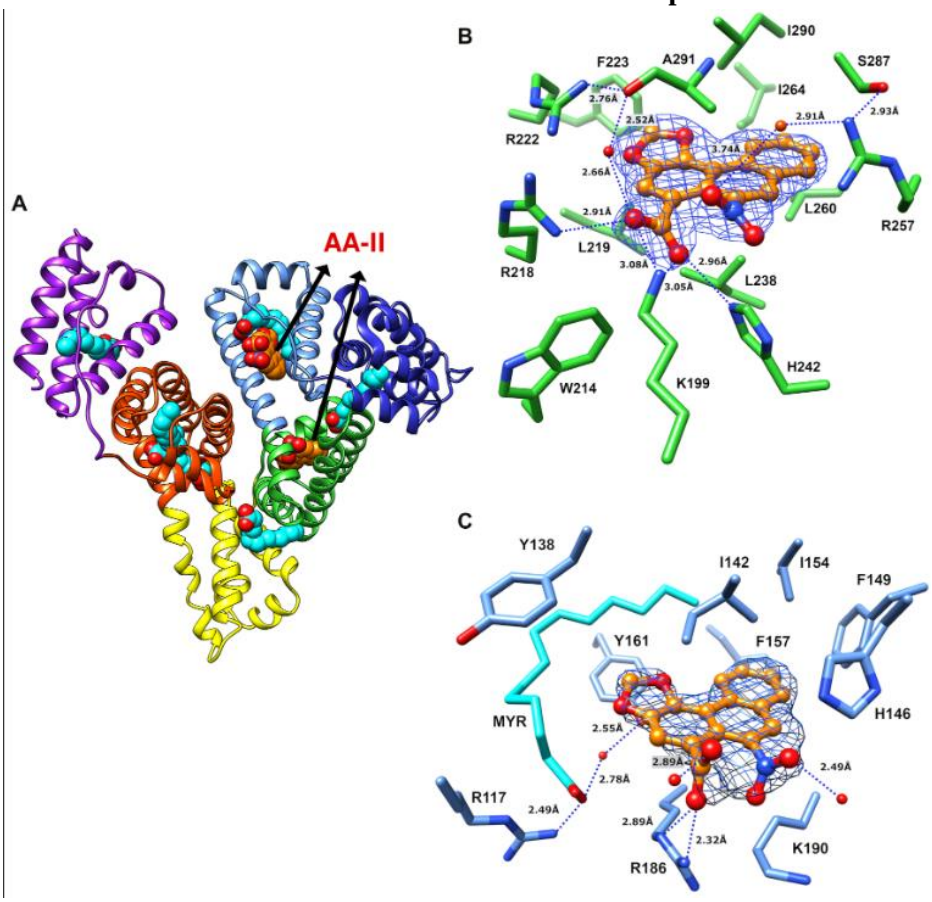

LEGEND: *Image A shows the overall structure of HSA with AA-II ligands bound to the subdomain IIA(FA7; green) and at the lip of subdomain IB(FA10; blue) adjacent to FA1(cyan). Image B shows the details of AA-II binding at subdomain IIA showing I290/A291 above and L238 below the aromatic plane. Image C shows a detailed view of AA-II binding at subdomain IB with a myristic acid molecule (cyan) occupying FA1 betwixt Y161 and Y138, where AA-II is located near H146. The 2Fo-Fc electron density maps of AA-II(blue mesh) in images B and C are fitted at 1.5sigma. Water molecules are shown as red spheres and hydrogen bonding distances shown as dotted lines.*

The HSAMYR/AA-II complex structure shows that AA-II interracts with FA7 at the spot originally occupied by a FA molecule, as seen in image A of figure 16. The conformation shows in the final crystal structure deposited (PDB ID 8RCO) and can be seen in image B of figure 16. Surprisingly data implies that two binding arrangements are possible within subdomain IIA, primarily the carboxylate and nitro groups of the AA-II are exchanged within the binding space, reflecting a 180 degree flip about the AA-II main axis

FIGURE 17: The Fo-Fc and 2Fo-Fc Electron Density Maps of AA-I/AA-II Bound in Subdomains IB and IIA

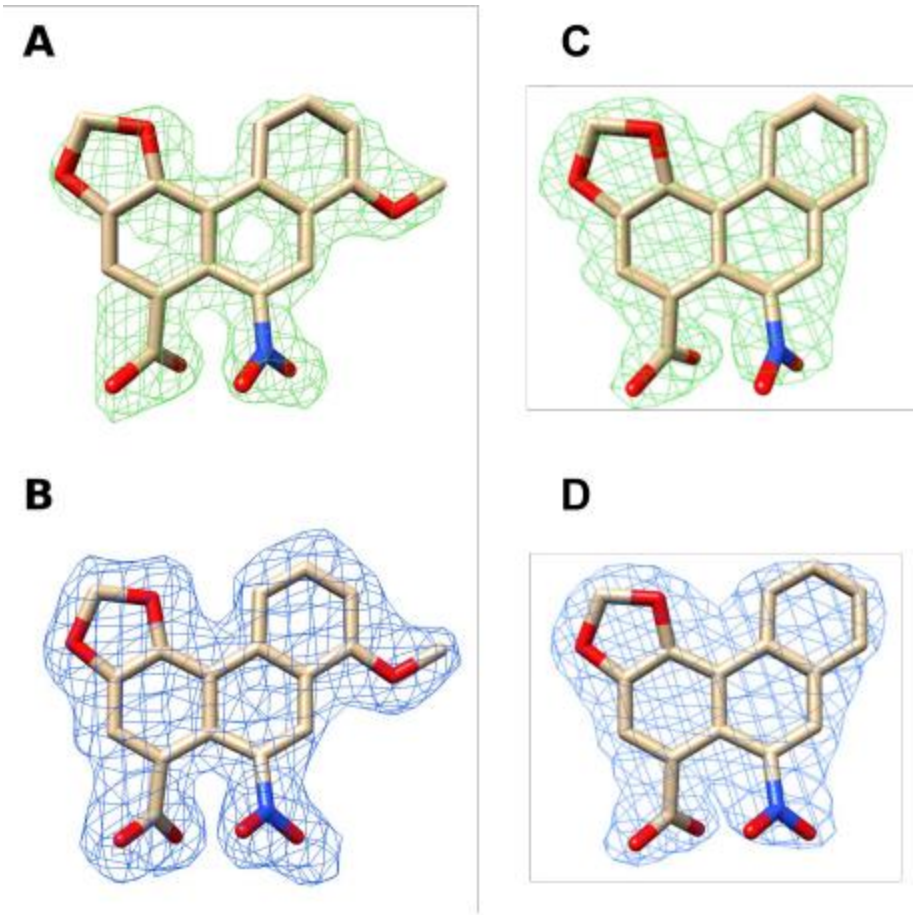

LEGEND: *The Fo-Fc, green mesh, and (image A) 2Fo-Fc, blue mesh. Image B is the electron density maps of AA-I when bound in subdomain IB fitted at 3sigma and 1sigma. The Fo-Fc, green mesh, and (image C) 2Fo-Fc, blue mesh. Image D shows the electron density maps of AA-II when bound in subdomain IIA fitted at 3sigma and 1.5sigma.*

It is possible that AA-II binds to drug site 1 (FA7) in both arrangements with distinct occupancies. When in the PDB ID 8RCO (preferred) arrangement, the aromatic area of AA-II is bound deeply in the space and creates hydrophobic interactions with nearby residues, as seen in image B of figure 16. The AA-II interacts with the I290/A291 and L238 from below and above the aromatic plane. The structural data obtained implies a common binding mode for AA-I/AA-II to HSA where the aromatic regions of the AA ligands create extensive hydrophobic interactions with lipophilic areas of HSA binding sites, and the carboxylate ans nitro groups are involved in favorable interactions. The AA-I in subdomain IB (FA1) and AA-II in subdomain IIA (FA7) look like the orientation of the myristic acids that had previously occupied those sites. AA-I binding to the FA1 site in subdomain IB can be characterized by ~467 of the total 487A^2 (~94%-98%) within the buried solvent-accessible surface area (SASA). Additionally, AA-II when bound in the subdomain IIA(FA7) is uncovered to the surrounding solvent by two slim channels and shows similar (~94%) surface area burial. When the AA-II is bound at the lip of subdomain IB, the amount of hidden SASA stays high (~93%) as seen in table 5, below.

TABLE 5: The SASA of AA Species Hidden Once Bound to HSA

Complex	Binding Site	Chain	Total SAS Å²	Buried SAS Å²	Buried SAS (%)
HSA_{MYR}/AA-I	IB	A	487.34	457.22	**93.8**
		B	485.82	478.58	**98.5**
HSA_{MYR}/AA-II	IIA	A	444.48	416.72	**93.8**
		B	444.80	419.44	**94.3**
	IB (Lip)	A	445.75	415.35	**93.2**
		B	445.93	413.02	**92.6**

LEGEND: *The analysis of HSAMYR/AA-I and HSAMYR/AA-II complexes show that hidden SASA exceeds 90% for the AA ligands that are bound to subdomains IB (AA-I/AA-II) and IIA (AA-II).*

To summarize, the highly specific binding of AA-I/AA-II to HSAMYR produces significant SASA burial as well as shielding from surrounding solution.

Discussion

The goal of this study was to identify and characterize molecular focus that govern the interactions betwixt aristolochic acids and their activated metabolites with HSA. Understanding these interactions is essential to understanding metabolic pathways of environmental compunds as well as thier mechanisms for distribution and carcinogenesis. Once this is understood, drug discovery, new treatmens, and new therapies can be obtained safely. The novel findings of this study can be summarized as follows; HSA extends the half-life and reactivity of labile N-sulfonyloxyaristolactam I, an active AA-I metabolite, which is assumed to expand the window of toxicity and ability to create DNA adducts. The HSA interactions with AAs and the metabolites are differentially influenced by the presence of fatty acids. The ITC profile monitoring the association of AA-I/AA-II with defatted HSA shows two binding sites that can be defined by micromolar affinities that usually confirm structural analysis. The high-res structures of HSAMYR, HSAMYR/AA-I, and HSAMYR/AA-II provide identification and structural clarity of AA interactions that are within the subdomain IB (AA-I/AA-II) and subdomain IIA (AA-II).

This study was imperfect, producing some optimal crystals and some less than optimal crystals. The study had mentioned that one of the limitations in binding studies are the use of bulk commercial HSA preps from pooled human plasma. The preps frequently have a significant ratio of cross-linked species because there is a singular CySH34 in the native HSA that is susceptible to several modifications. Also, CySH34 is prone to covalent bonding with electrophilic species of different xenobiotics. The modified species of albumin will form crystals that tend to diffract poorly. A next-step in identifying and characterizing molecular forces that govern the interactions between AAs and their activated metabolites with HSA could be using an unmodified species of albumin.Thanks to the high-res crystal structure (being the highest-res crystal structure recorded of AAs bound to HSA), the mechanisms, binding sites, and molecular interactions of AA-I/AA-II with HSA are more understood. While there is still more work to do in refining the data and growing more optimal crystals (as some were optimal and some where not). Now it is possible to discover drugs and some new treatments/therapies using AA-I/AA-II bound to HSA relatively safely. Although it will likely take an additional study or more, this study was a huge step forward.

Sources

- Biol.4892/5892 Crystallography and Structural Bioinformatics (class slides), University of Massachusettes Lowell and Professor Hwai-Chen Guo, 2025
- Biophysical Chemistry, Part II, Charles Cantor and Paul R. Schimmel, W.H. Freeman and Company, 1980
- Methods in Enzymology, Vol. 276 and 277: Macromolecular Crystallography Parts A and B, Charles W. Carter, Jr. and Robert M. Sweet eds., Academic Press, 1997
- MyBib Contributors. (2019, May 26). *APA Citation Generator – FREE & Fast – (6th Edition, 2019)*. MyBib. https://www.mybib.com/tools/apa-citation-generator
- Protein Crystallography, T.L. Blundell and L.N. Johnson, Academic Press, 1976
- Sergei Pomyalov, Minetti, C. A., Remeta, D. P., Radha Bonala, Johnson, F., Zaitseva, I., Iden, C., Urszula Golebiewska, Breslauer, K. J., Shoham, G., Sidorenko, V. S., & Grollman, A. P. (2024). Structural and Mechanistic Insights into the Transport of Aristolochic Acids and their Active Metabolites by Human Serum Albumin. *Journal of Biological Chemistry*, *300*(7), 107358–107358. https://doi.org/10.1016/j.jbc.2024.107358
- Structural Bioinformatics, Jenny Gu and Philip E. Bourne, Wiley-Blackwell, 2009
- X-Ray Structure Determination, 2nd ed., George H. Stout and Lyle H. Jensen, John Wiley and Sons, 1989
- Understanding bioinformatics, Marketa Zvelebil and Jeremy O. Baum, Garland Science, 2008